coatings

MDPI

Article

Capturing the Competing Influence of Thermal and Mechanical Loads on the Strain of Turbine Blade Coatings via High Energy X-rays

Albert Manero II [1], Kevin Knipe [1], Janine Wischek [2], Carla Meid [2], John Okasinski [3], Jonathan Almer [3], Anette M. Karlsson [4], Marion Bartsch [2,*] and Seetha Raghavan [1]

1 Department of Mechanical and Aerospace Engineering, University of Central Florida, 4000 Central Florida Blvd., Orlando, FL 32816, USA; albert@limbitless-solutions.org (A.M.II); kknipe27@gmail.com (K.K.); Seetha.Raghavan@ucf.edu (S.R.)

2 German Aerospace Center, Institute of Materials Research, Linder Höhe, 51147 Köln, Germany; janine.wischek@dlr.de (J.W.); Carla.Meid@dlr.de (C.M.)

3 X-Ray Science Division, Advanced Photon Source, Argonne National Laboratory, Argonne, IL 60439, USA; okasinski@aps.anl.gov (J.O.); almer@aps.anl.gov (J.A.)

4 Washkewicz College of Engineering, Cleveland State University, 2121 Euclid Ave, Cleveland, OH 44115, USA; a.karlsson@csuohio.edu

* Correspondence: Marion.Bartsch@dlr.de; Tel.: +49-2203-601-2436

Received: 12 July 2018; Accepted: 30 August 2018; Published: 10 September 2018

Abstract: This paper presents findings of synchrotron diffraction measurements on tubular specimens with a thermal barrier coating (TBC) system applied by electron beam physical vapor deposition (EB-PVD), having a thermally grown oxide (TGO) layer due to aging in hot air. The diffraction measurements were in situ while applying a thermal cycle with high temperature holds at 1000 °C and varying internal air cooling mass flow and mechanical load. It was observed that, during high temperature holds at 1000 °C, the TGO strain approached zero if no mechanical load or internal cooling was applied. When applying a mechanical load, the TGO in-plane strain (e22) changed to tensile and the out of plane TGO strain (e11) became compressive. The addition of internal cooling induced a thermal gradient, yielding a competing effect, driving the e22 strain to compressive and e11 strain to tensile. Quantifying TGO strain variations in response to competing factors will provide a path to controlling the TGO strain, and further improving the lifetime assessment and durability design strategies for TBC systems.

Keywords: thermal barrier coatings; thermal gradient mechanical load; synchrotron

1. Introduction

Jet engine turbine blades are exposed to increasingly extreme conditions in order to advance both efficiency and performance for air breathing engines. Driven by the need to improve thermal efficiency, turbine inlet temperatures have been elevated by 500 °C over the past decades [1]. In an effort to maintain and increase the longevity of the superalloy blades, internal cooling flows have been introduced for generating thermal gradients. The internal flow, along with architected thermal barrier coatings (TBCs), reduces the temperature on the superalloy but induces a thermal gradient over the coating system [2]. Typically, TBCs for aircraft engine blades comprise a superalloy load bearing substrate with an yttria-stabilized zirconia (YSZ) coating deposited via electron-beam physical vapor deposition (EB-PVD). This deposition method is used for generating layers with a columnar structure, resulting in the necessary strain tolerance during thermal and mechanical cyclic loading in service. As the YSZ topcoat is permeable to oxygen, a metallic layer, such as NiCoCrAlY, is applied onto the substrate for protecting it against oxidation by forming a dense alumina layer, known as the

thermally grown oxide (TGO). During the deposition of YSZ, an initial TGO is formed, typically less than 1 micron thick. However, during the life of the TBC, the TGO grows as it is exposed to elevated temperatures during service. The growth rate is non-linear in nature and influences the resulting mechanical behavior of the coating system in response to complex loading conditions. It has been observed that the oxide scale has a critical role in the failure mechanisms of the coating system, and this has been of great interest of study (e.g., [3–11]) to understand the damage process and predict the lifetime of the coating system.

Most research has been conducted on flat coupon or cylindrical specimens to evaluate the effect of thermal load cycles (e.g., [7,12]). These tests have been very effective for ranking different coating systems with respect to performance under the respective experimental testing conditions, yet they also highlight the need for more advanced in-situ measurements that provide strain data within the coating layers under loads close to the complex service conditions to support theory and simulation efforts [13]. By introducing mechanical loading in addition to thermal cycling [14], it was possible to separate the effects of mechanical and thermal load, as well as to provide a lifetime model based on calculated strain in the TGO as a function of thermal mismatch and elastic material properties. The inclusion of induced thermal gradients, such as air cooling on the leeward surface of a sample contrasted with torch heating [15–17] or radiation heating [18], has advanced the characterization and deciphering of TBC behavior under thermal loading. Further work with tubular specimens and simultaneous thermal and mechanical loading and adding a thermal gradient has been performed to apply more realistic loading conditions in laboratory testing [19], resulting in spallation and specific crack patterns enhancing spallation [20]. Computational analyses of the experimental findings in [20] provided reasonable explanations for the observed damage features [21,22]; however, for validation of the numerical results, in situ measurement of the strain in all layers of the TBC system was needed. The technique used in [19] has been adapted in [23–25] to reveal, by in situ X-ray diffraction, the role of loading variations on the strain of the different layers of a TBC coating system. However, thus far, strain evaluation for the TGO, which is governing the TBC failure in most cases, has been incomplete due to the difficulties in analyses of the diffraction pattern coming from the exceptionally thin layer.

To understand both the effect of the loading condition, and to isolate their influence on the strain of the employed coating layers, in-situ measurements are required. Time dependent behaviors for multi-layer coating systems can be observed with the application of high energy X-ray diffraction from a synchrotron source in in-situ testing [24–28]. These high available energies and flux result in short collection times and high spatial resolution for simultaneous non-destructive analysis of multiple constituents and layers. This has been utilized to quantify the effect for a multi-variable assessment and to elucidate the conditions' influence on the failure mechanisms that plague TBCs.

2. Experimental

In this study, in-situ X-ray diffraction data of tubular coated and aged specimens were collected under multivariable loading conditions capturing their influence on the strain of the thermally grown oxide layer in a TBC system. A multivariable analysis has been conducted to determine the role and magnitude of the following variables: mechanical (axial) loading, external temperature, and internal cooling air flow. This is represented in Figure 1 and is further detailed in this section.

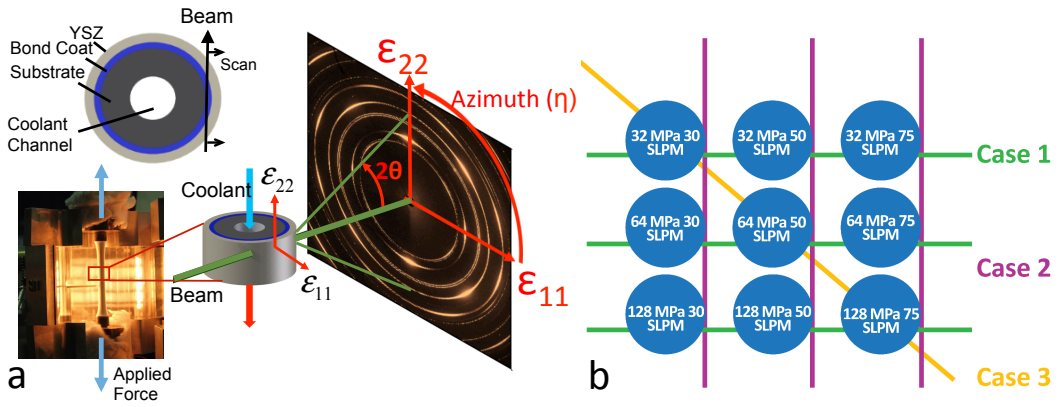

Figure 1. (**a**) view of specimen with attached thermocouple placed in furnace and schematic of experimental methodology with nomenclature of determined strain. (**b**) Multivariable matrix for Case 1 (constant load, variable flow in standard liters per minute), Case 2 (constant flow, varying mechanical loading), and Case 3 (extrema loading conditions).

The experimental study focused on the aged TBC specimens with a sufficiently thick oxide scale for strain analyses by X-ray diffraction. Sample design is elaborated in the Sample manufacturing section. Experiments were designed to provide a multi-variable assessment of the role and magnitude of the following variables: mechanical (axial) loading, external temperature, and internal cooling air flow. To understand the influence of the variables, three cases were investigated (see Figure 1).

- Case 1: constant mechanical loading with variable internal cooling
- Case 2: constant internal cooling with variable mechanical loading
- Case 3: extrema of variable loading as follows:
  - Low mechanical loading/low flow
  - Mid-range mechanical loading/mid-range flow
  - High mechanical loading/high flow

These cases were conducted for a consistent thermal loading profile over a 60-min test, and are elaborated on herein. The testing methodology has been evaluated and documented in respective literature [19,20,23].

Individual cycles with thermal and mechanical loading: In-situ strain measurements were conducted with variations in both mechanical loads and internal cooling flow for representative cycles. Testing conditions included a 20 min ramp from ambient to 1000 °C, a high-temperature hold for 20 min, and a decrease to ambient for 20 min. Additionally, internal cooling air flow was implemented, with a mass flow between 0 and 100 Standard Liters Per Minute (SLPM). Figure Sup1 represents the conditions employed on the specimen, during which depth strain measurements over the coating thickness were conducted. Cycles with superimposed constant mechanical loads providing a nominal tensile stress of 32, 64, and 128 MPa were paired with flow variations of 0, 30, 50, and 75 SLPM. This produced a large matrix of results shedding light on material properties as a function of temperature, mechanical loading (stress), and dwell time [24,25].

Increasing flow: Figure Sup1b details the "effect of flow" experiment. In an effort to identify the variation in strain for the coating system at a high temperature with respect to internal cooling, this experiment was conducted. After the surface of the coating system was held at 1000 °C, internal cooling was turned on and increased in small steps accompanied by in-situ strain measurements. Measuring through the depth of the coating, the influence of the increasing flow on the strain of the TGO was observed.

2.1. Sample Manufacturing

This experiment used a single tubular dog bone shaped specimen specified in [19–21], as shown in Figure 1. The substrate was an Inconel 100 directionally solidified alloy, with an inner diameter of 4 mm and outer diameter of 8 mm. The bond coat of NiCoCrAlY was deposited via EB-PVD to a thickness of 118 $\pm$ 4 microns, on which adhered a partially stabilized zirconia top coat with 7–8 wt% yttria content at a thickness of 211 $\pm$ 4 microns. The specimen had been aged at uniform temperature in a furnace for 304 h at 1000 °C in air to develop the thermally grown oxide to a thickness sufficient for X-ray diffraction analyses. Referring to data experimentally obtained in a previous study [21], the pre-aged specimen had a 4 micron thick TGO. The comparably minimal number of cycles added by the experimental matrix had negligible effects on TGO composition and growth.

2.2. Synchrotron Diffraction Measurements under Loading

X-ray diffraction patterns were obtained using the high-energy X-ray diffraction technique offered at the 1-ID Beamline at the Advanced Photon Source (APS) at Argonne National Laboratory (ANL). This high-energy XRD technique employed monochromatic transmission geometry fitted with a GE 41RT 2048 $\times$ 2048 pixels area detector to measure diffracted X-ray intensities for further determining volume fraction of phases present and crystallographic texture qualities in each phase of the polycrystalline material. The beamline was operated at 65 keV with CuK (0.7125 Å) radiation. The total X-ray flux was 1012 photons/s. To obtain precise and accurate information from the scans, calibration of the detector position and orientation with respect to the incident beam was performed using ceria powder. The sample to detector distance yielded crystallographic range of d-spacings of 1.3 to 3.5 Å. Scans were taken from the edge of the sample working towards the center with beam size of 300 microns height (parallel to load axis) and 30 microns width, with a 50 micron step size. Scanning tangentially with this beam, the radial thickness of the TGO layer is treated as a near linear slice compared to the much larger radial thickness of the cylinder.

High-temperature in-situ measurements were taken using a set up including an 8 kW infrared (IR) heating chamber, Type E4, and control system (Precision Control Systems Inc., Eden Prairie, MN, USA). Radiation was applied by four quartz short IR wavelength lamps in a hinged clam-shell style chamber focused onto the specimen in the center line of the furnace by way of elliptical mirrors. The chamber has four polished water-cooled aluminum reflectors to focus the IR energy on the target located in the center of the camber. The chamber includes the four 2 kW T3 lamps, protective quartz windows and dripless water connectors. The control system regulates the voltage to the lamps and includes a temperature controller that was configured for a type "S" thermocouple for the high temperature experiments performed here. Samples were heated at ramp rates of 50 K per min to temperatures up to 1000 °C. High-performance computing (HPC) batch correction was used to convert area detector data and MATLAB was used for subsequent processing.

2.3. Statistical Analysis

With X-ray diffraction, there is an intrinsic sensitivity challenge for measuring extremely small strains. For synchrotron diffraction with 2D area detectors, the resolution limits are extremely precise with values in the range of 10^{-4} mm/mm being deciphered. The uncertainty increases when approaching zero strain and decreases with increasing strain. As such, values of certain response curves at high temperature in the range of 10^{-5} mm/mm are considered effectively zero. In Figure 2c,f, there are distinct points with no error bars where the values of the strain are too close to zero to overcome the minimal noise in the system. For slightly larger strain in the range of 10^{-4}, this is not an issue.

Each resulting data point is a fit of an eccentric ellipse from the Debye rings produced by that crystallographic plane under strain. For the alumina scale, the (116) plane was selected for strain analysis as it had the minimum convolution with the bond coat peaks. The strain free reference approximation was modeled using room temperature lattice parameters with single crystal data from literature [29] since variations are minimal for the material. Lattice dependent X-ray elastic constants were calculated via the DECCalc software [30] and used to estimate the invariant radius and azimuthal angle. Note that this is the reference angle at which zero deviatoric strain occurs. At high temperature, considerable thermal expansion along with bond coat phase change due to formation of precipitates was observed. Scans across the thickness reveal low intensity characteristic alumina diffraction peaks. However, further scans oriented medially probe bond coat precipitations, which can convolute and obscure diffraction peaks of the thin oxide layer. To mitigate this, a Fourier fitting method was employed to overcome fitting challenges where segments of the oxide were obscured by the bond coat. Distinguishing between the two overlapping phases was made easier by the texturing or roping of the bond coat phases as well as by its dramatic intensity in comparison to the oxide. Some of these considerations are show in Figure A2b.

Error bars are generated for the average radius for all of the specific azimuthal bins segmented around the Debye ring. The full discretized ring is fit by a Fourier routine that considers all points. Confidence intervals are constructed for 90% confidence, providing an understanding of the variation for each strain fit. Error bars represent the maximum and minimum confidence range for each measurement point. For outliers multiple standard deviations away from the average, a bisquare robust regression is used to weight their influence on the full fitting curve. This is particularly effective for issues with bond coat peak interference, as shown in Figure A2a, where azimuthal bins will fit neighboring higher intensity bond coat peaks and miss the obscured oxide scale peak. The more closely the data matches the Fourier sinusoidal shape, the stronger the predictive nature of the routine becomes. As such, for strong signals with small areas of obscured data including textured or interfering data segments, the routine is very effective for capturing the appropriate fits. An R-squared value for each fit is determined and used to evaluate the goodness of fit for every measurement point.

Examining the effect of increasing internal cooling flow at high temperature hold, it was shown that the strain response is non-linear which highlights that the variation between 30, 50, and 75 SLPM entails not a purely linear increase in effect due to non-linear heat transfer and flow properties for the internal pipe flow. This may be the cause of some of the strain response profiles having minimal variation comparing the 50 and 75 SLPM variables. The trends follow an expected non-linear response, which results from the heat transfer coefficient being non-linear for transitioning internal pipe flow [27,28]. This is seen to level out the resulting strain response between 40 and 60 SLPM.

Throughout this experimental work, the aim was to observe statistically relevant trends and influences, while understanding the inherent uncertainty from such a complex real time experiment. For example, due to the time associated with scanning through the 10 measurement zones, the final strain measurement (time) for the oxide layer at high temperature hold can move considerably. This results in missing information between the last measurement at the high temperature hold and the first measurement (time) during thermal ramp down. Consequently, the variables influence on the ramp down strain slope needs to be evaluated for the next continuous two strain measurements. This is shown in Figure 2a,e (32 MPa curve).

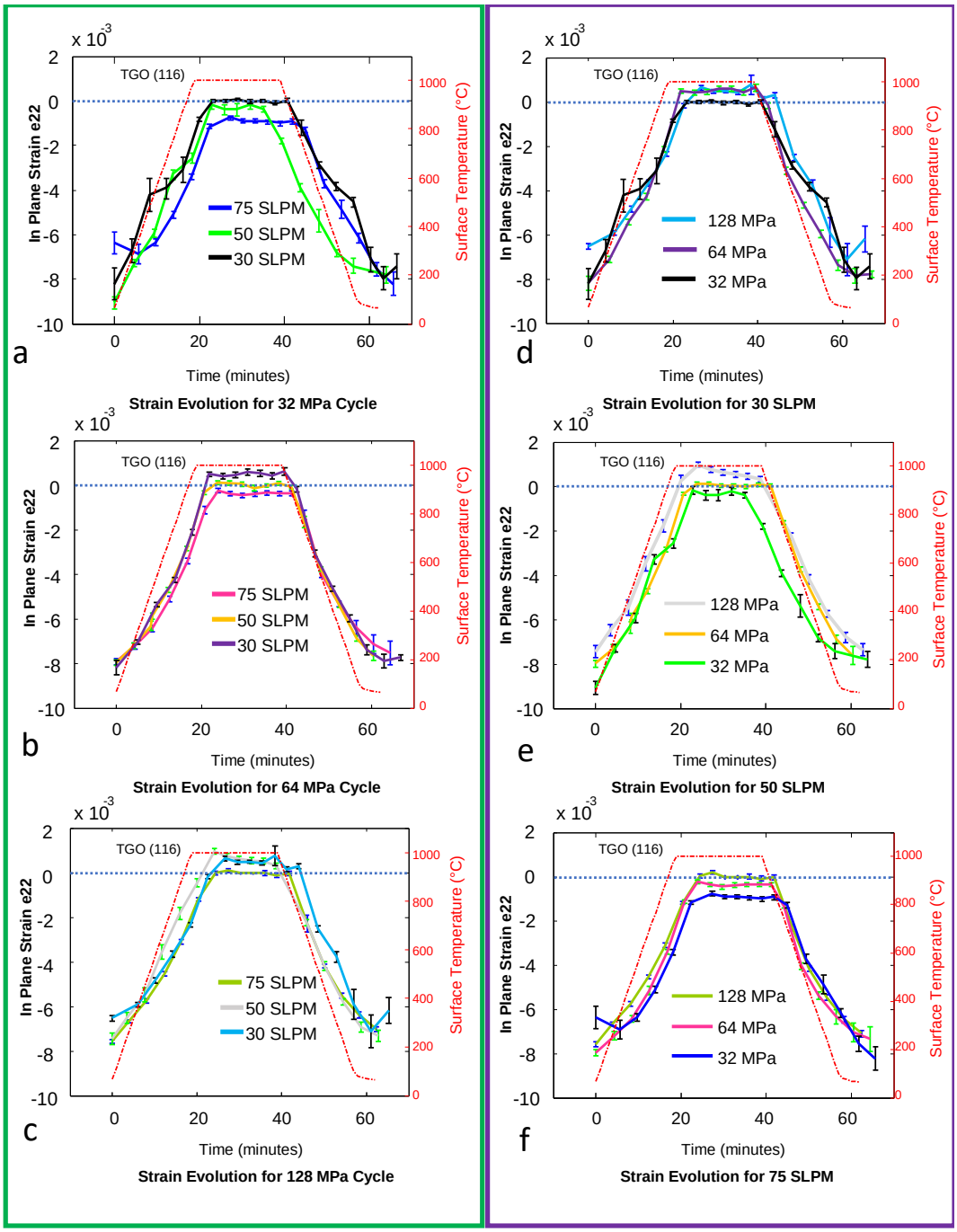

Figure 2. TGO e22 strain response over thermal cycle for constant mechanical load with varying flow (**a**–**c**); and replotted to show constant flow with varying mechanical loading (**d**–**f**).

3. Results and Discussion

The experiments produced high-resolution 2D diffraction data yielding the constituent strain data of the multi-layer system. A full multi-variable testing procedure was performed to understand and quantify the influence of the mechanical loading, thermal loading, and internal cooling testing parameters. An image of the testing is presented in Figure 1. Of primary importance was the comparison of constant mechanical load with variable flow and constant flow with variable mechanical loading. Comparing the resulting nine individual full system tests, Figure 2 was produced for

the primary comparison of the axial in plane TGO strain e22 parallel to mechanical load direction. From these findings, the influences of the multiple variables on the oxide scale can be identified.

- Increasing internal cooling flow, at high temperature holds and constant mechanical load, results in decreasing strain, e22. That is, for the cases of lower mechanical constant load, the strain becomes more compressive, while for higher constant mechanical load, the strain goes from tensile to compressive. This is clearly seen in Figure 2a–c. This is mainly because the internal air cooling increases the thermal gradient across the specimens wall, resulting in constraining the expansion of the specimen, and a compressive TGO strain. Further, although the role of increased internal flow from low to high flow is distinct, the midrange flow measurement (50 SLPM) shows decreased confidence and sensitivity as elaborated in Section 2.3.
- Increasing mechanical loading, at constant flow and constant external temperature, will push the oxide scale into tension. This is of specific interest at high temperature holds, where sufficient axial loading can take the oxide scale from compression or near zero strain and pull it into tension. This is shown in Figure 2c and further visible in Figure 2d–f. In previous work [21], it has been shown that further tensile stresses may form due to creep relaxation over cyclical loading. However, when mechanical loading is combined with internal cooling, the variables compete and the resulting superposition is reflected.
- The response to high temperature hold depends on the strain level resulting from the combined applied mechanical load and internal cooling air flows. When reaching a high tensile strain, significant strain relaxation is observed, which can be seen clearly in Figure 2. When the strain during hold is compressive, a slight increase of compressive strain occurs, as displayed in Figure 2a,f. These observations can be explained by considering the two competing mechanisms of creep relaxation and accumulation of growth strain as investigated via numerical analyses in [21]. At high temperature it is assumed that TGO growth results not only in thickening of the TGO but also in depositing material at grain boundaries of the TGO causing increase of in-plane compressive strain, as discussed in the literature [8,9]. While the growth strain always increase the compressive strain, creep relaxation is actively driving the strain always towards zero. Thus, at high tensile strain level creep relaxation and growth strain are acting both to reduce the strain. In contrast, at high compressive strain level, creep relaxation and growth strain are counteracting. Depending on creep parameters, growth rate, and yield strength of the TGO, an equilibrium strain or stress will be reached after certain hold time. At strain levels close to zero, the sensitivity of synchrotron strain measurements is decreased due to superposed signal noise. This is further discussed in the statistical section.
- Next, consider the influence of internal flow on the TGO strain response during thermal ramping. During thermal cycling, the surface heating by the radiation furnace introduces a transient thermal gradient over the specimen wall, which—without internal cooling—would vanish during hold at high temperature. The transient thermal gradient results in a delay of TGO strain response with respect to the surface temperature. Superposing an internal cooling air flow increases the time lag in strain response, which is visible when comparing the strain evolution at thermal ramp up in Figure 2f with that in Figure 2d,e.

By taking Case 3 as detailed in Figure 1, i.e., combining mechanical loading and internal cooling in low–low, mid–mid, and high–high conditions, the strain level during hold was kept close to zero. Figure 3a,b shows the strain evolution for both in plane parallel to applied load and out of plane (e22 and e11). A schematic is presented in Figure A1a,b further elaborating the loading conditions and comparison of in plane and out of plane strains. Of particular importance was that variables' influences during high temperature hold are seen to compensate each other. This is most visible in both the e22 and e11 response in Figure 3a,b as all the response curves show effectively zero strain during high temperature hold. However, such influence compensation only holds true for mid and high applied surface temperatures, while variation is still seen in the low temperature strain response

(below 800 °C). It can be inferred that, at low temperatures, applied mechanical loading dominates over the internal cooling variable's influence on the resulting strain, because at low temperatures the thermal gradient is lowered.

In an effort to more completely understand the individual variables' influences, additional experiments were designed as shown in Figure A1b. While at a constant surface temperature of 1000 °C, internal cooling flow was gradually increased from 0 SLPM to 85 SLPM. No mechanical load was applied in these experiments. The resulting in plane and out of plane (e22 and e11) TGO strain results are plotted in Figure 4a,b, and the influence of increasing coolant flow can be quantified. The trends follow an expected non-linear response, which results from the heat transfer coefficient being non-linear for transitioning internal pipe flow from laminar to turbulent [31,32]. This is seen to level out the resulting strain response between 40 and 60 SLPM. For the e22 response, the maximum flow is observed to result in -1.5×10^{-3} (compressive) strain. Conversely, for e11 response, the maximum flow increases the strain to 4×10^{-4} (tensile).

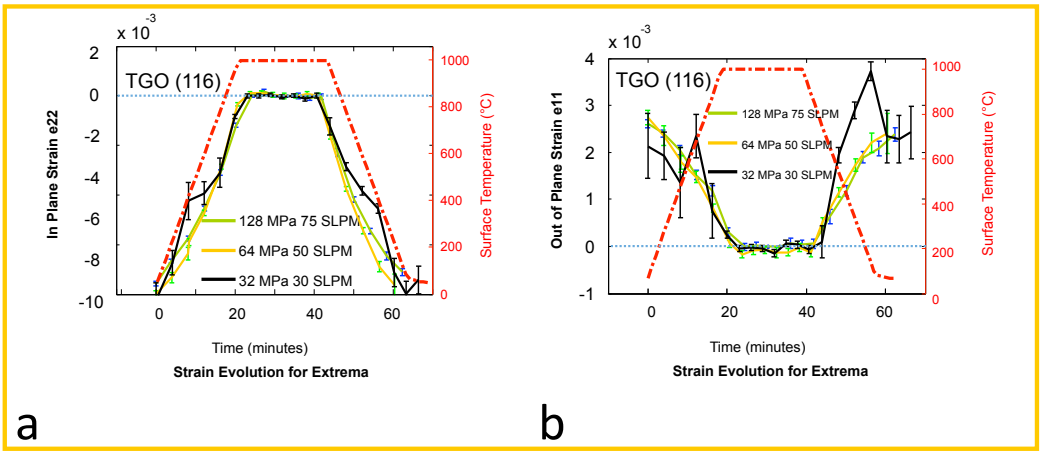

Figure 3. Extrema plots to show strain evolution at low, medium, and high mechanical load and respective internal flow: (**a**) in plane strain; and (**b**) out of plane strain.

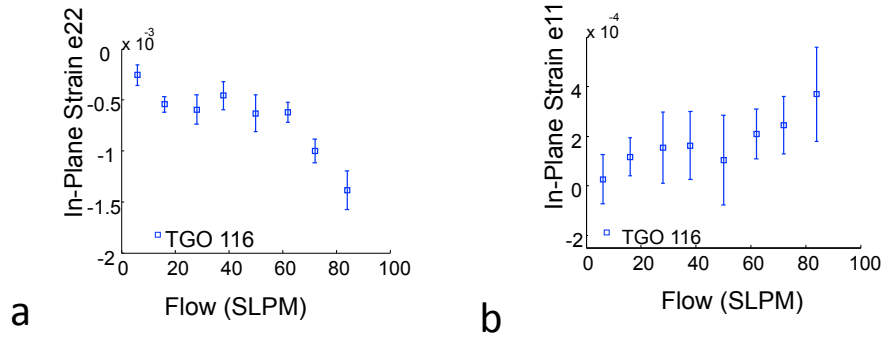

Figure 4. Variation of e22 (**a**) and e11 (**b**) TGO strain at 1000 °C high temperature hold as a function of internal coolant flow.

The primary influences are summarized qualitatively in Figure 5 and summarized for their implications on durability. Unique to this study is the multi variable analysis, showcasing the interaction between different variables. Herein, it is discussed that the internal cooling has an influence to cause a lag in strain response to increasing external temperature. It was further shown that higher mechanical loading and internal cooling flow have a converse influence on the TGO strain.

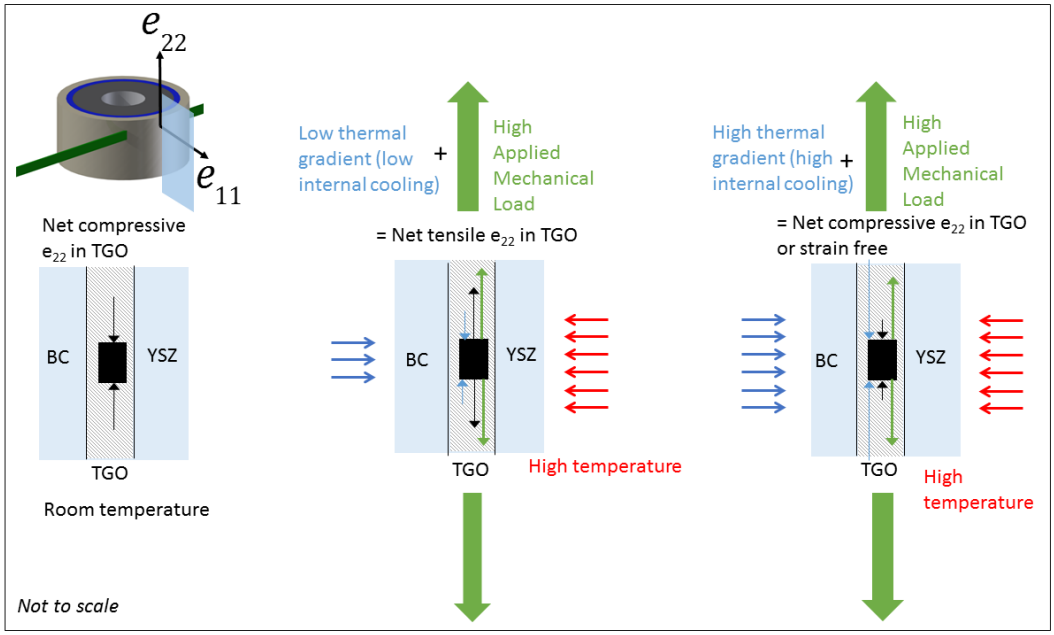

Figure 5. Schematic illustrating the competing effects of applied loads and thermal gradients.

4. Conclusions

The multi-variable study provided the ability to understand the influence and to quantify the effects of mechanical loading, internal cooling, and externally applied thermal loading. The major outcome is to quantitatively determine the influence of the selected variables on the TGO strain, which has significant implications in the design of these coatings for durability. Specifically, the accomplishments can be highlighted as:

- Quantifying the change in tensile strain magnitude at high temperature due to variable applied mechanical loading;
- Quantifying the non-linear in plane and out of plane TGO strain variation due to increased internal cooling flow rates;
- Demonstrating the competing nature of external mechanical loading and the effectiveness of internal cooling flow rates, suggesting that tuning local internal flow rates across a turbine blade could mitigate potential high tensile strains at operating temperatures.

The breakthrough of establishing the competing influences of applied loads and thermal gradients on the internal strains lies in identifying critical cycle scenarios that can lead to tensile strains within the TGO which have a negative impact on durability. This work offers the capacity to use the measurement results to establish design strategies for internal cooling that would prevent the generation of tensile strains within the TGO, potentially avoiding specific damage mechanisms.

The significance of this study is that of quantifying how realistic loading influences the strain state in the oxide scale, which is critical to understanding the failure mechanisms of the coated system. The results are consistent with trends and hypotheses established by previous model experiment and simulation. The results and enhanced understanding allows for advancing the life prediction for a turbine blade and coating system, where the internal cooling, external temperatures, and centrifugal loading vary. The approach has the ability to revolutionize design strategies for durability enhancement for coated aircraft turbine blades.

Author Contributions: Conceptualization, A.M.K., M.B., J.A., and S.R.; Methodology, A.M.II, K.K., J.A., J.O., A.M.K., C.M., J.W., M.B., and S.R.; Formal Analysis, A.M.II and K.K.; Investigation, A.M.II, K.K., C.M., and J.W.; Resources, J.A., J.O., A.M.K., M.B., and S.R.; Data Curation, A.M.II, K.K.; Writing-Original Draft Preparation, A.M.II; Writing-Review and Editing, A.M.II, A.M.K., C.M., J.A., J.O., J.W., K.K., M.B. and S.R.; Visualization, A.M.II and K.K.; Supervision, J.O., J.A., M.B. and S.R.; Project Administration, S.R. and M.B.; Funding Acquisition, S.R. and M.B.

Funding: This material was based upon work supported by the National Science Foundation grants OISE 1157619, CMMI 1125696, by the German Science Foundation (DFG) grant No. SFB-TRR103, Project A3, and the Fulbright Academic Grant (Grant No. 34142765). Use of the Advanced Photon Source, an Office of Science User Facility operated for the US Department of Energy (DOE) Office of Science by Argonne National Laboratory, was supported by the US DOE under contract No. DE-AC02- 06CH11357.

Conflicts of Interest: The authors declare no conflict of interest.

Appendix A

The following supplementary figures display the loading profiles and the strain analysis methods used in the study.

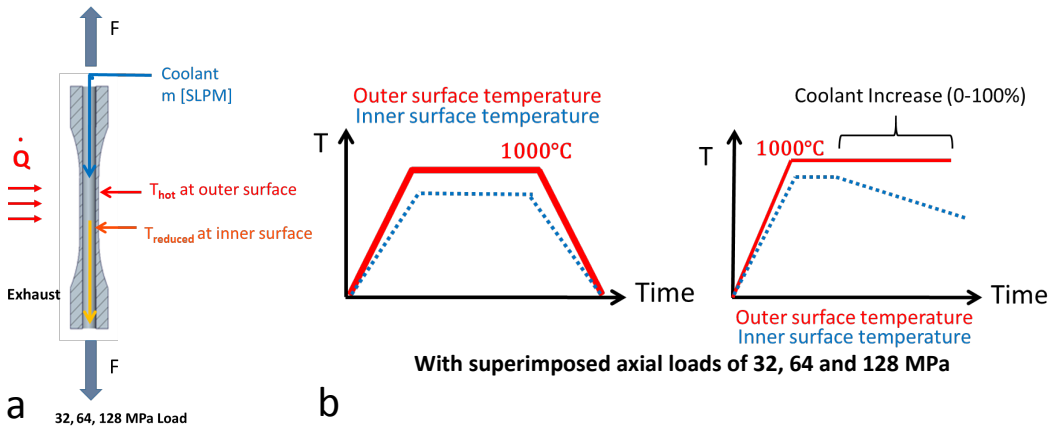

Figure A1. Experimental setup: (**a**) application of mechanical loading; and (**b**) thermal loading profiles for cycle testing and flow testing [23–25].

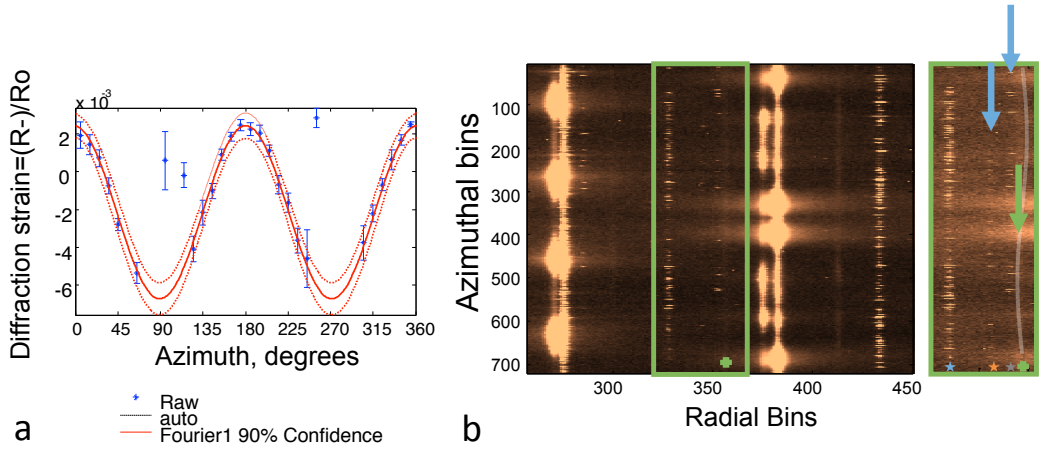

Figure A2. Strain analysis and fitting challenges for transformed Debye rings: (**a**) fitting challenges for strain response with bond coat overlap over alumina peak, with representations of in plane (e22) and out of plane (e11) strain data; and (**b**) examination of transformed Debye rings with precipitates obscuring oxide layer ring. Secondary peaks marked in blue interfere with faint TGO peak marked in green.

References

1. Dorfman, M.; Stapgens, M.; Medrano, J.; Sporer, D. Takeoff with advanced coatings: Improving thermal protection through new material solutions. *Sulzer Tech. Rev.* **2013**, *3*, 8–12.
2. Reed, R. *The Superalloys: Fundamentals and Applications*; Cambridge University Press: Cambridge, UK, 2006.
3. Padture, N.P.; Gell, M.; Jordan, E.H. Thermal barrier coatings for gas-turbine engine applications. *Science* **2002**, *296*, 280–284. [CrossRef] [PubMed]
4. Busso, E.; Evans, H.; Qian, Z.; Taylor, M. Effects of breakaway oxidation on local stresses in thermal barrier coatings. *Acta Mater.* **2010**, *58*, 1242–1251. [CrossRef]
5. Evans, A.; Mumm, D.; Hutchinson, J.; Meier, G.; Pettit, F. Mechanisms controlling the durability of thermal barrier coatings. *Prog. Mater. Sci.* **2001**, *46*, 505–553. [CrossRef]
6. Eberl, C.; Wang, X.; Gianola, D.S.; Nguyen, J.T.D.; He, M.Y.; Evans, A.G.; Hemkerz, K.J. In situ measurement of the toughness of the interface between a thermal barrier coating and a Ni alloy. *Am. Ceram. Soc.* **2011**, *94*, 120–127. [CrossRef]
7. Gell, M.; Eric, J.; Krishnakumar, V.; McCarron, K.; Barber, B.; Sohn, Y.H.; Tolpygo, V.K. Bond strength, bond stress and spallation mechanisms of thermal barrier coatings. *Surf. Coat. Technol.* **1999**, *120*, 53–60. [CrossRef]
8. Harvey, M.; Courcier, C.; Maurel, V.; Rémy, L. Oxide and TBC spallation in β-NiAl coated systems under mechanical loading. *Surf. Coat. Technol.* **2008**, *203*, 432–436. [CrossRef]
9. Karlsson, A.M.; Hutchinson, J.; Evans, A. The displacement of the thermally grown oxide in thermal barrier systems upon temperature cycling. *Mater. Sci. Eng. A* **2003**, *351*, 244–257. [CrossRef]
10. Karlsson, A.M.; Hutchinson, J.; Evans, A. A fundamental model of cyclic instabilities in thermal barrier systems. *J. Mech. Phys. Solids* **2002**, *50*, 1565–1589. [CrossRef]
11. Lipkin, D.; Clarke, D. Measurement of the stress in oxide scales formed by oxidation of alumina-forming alloys. *Oxid. Met.* **1996**, *45*, 267–280. [CrossRef]
12. Schulz, U.; Leyens, C.; Fritscher, K.; Peters, M.; Saruhan-Brings, B.; Lavigne, O.; Dorvaux, J.M.; Poulain, M.; Mévrel, R.; Caliez, M. Some recent trends in research and technology of advanced thermal barrier coatings. *Aerosp. Sci. Technol.* **2003**, *7*, 73–80. [CrossRef]
13. Marino, K.A.; Hinnemann, B.; Carter, E.A. Inaugural article by a recently elected academy member: From the cover: Atomic-scale insight and design principles for turbine engine thermal barrier coatings from theory. *Proc. Natl. Acad. Sci. USA* **2011**, *108*, 5480. [CrossRef]
14. Wright, P.K. Influence of cyclic strain on life of a PVD TBC. *Mater. Sci. Eng. A* **1998**, *245*, 191–200. [CrossRef]
15. Traeger, F.; Vaßen, R.; Rauwald, K.H.; Stöver, D. Thermal cycling setup for testing thermal barrier coatings. *Adv. Eng. Mater.* **2003**, *5*, 429–432. [CrossRef]
16. Vaßen, R.; Cernuschi, F.; Rizzi, G.; Scrivani, A.; Markocsan, N.; Östergren, L.; Kloosterman, A.; Mevrel, R.; Feist, J.; Nicholls, J. Recent activities in the field of thermal barrier coatings including burner rig testing in the European Union. *Adv. Eng. Mater.* **2008**, *10*, 907–921. [CrossRef]
17. Drexler, J.M.; Aygun, A.; Li, D.; Vaben, R.; Steinke, T.; Padture, N.P. Thermal-gradient testing of thermal barrier coatings under simultaneous attack by molten glassy deposits and its mitigation. *Surf. Coat. Technol.* **2010**, *204*, 2683–2688. [CrossRef]
18. Kitazawa, R.; Kakisawa, H.; Kagawa, Y. Anisotropic TGO morphology and stress distribution in EB-PVD Y_2O_3-ZrO_2 thermal barrier coating after in-phase thermo-mechanical test. *Surf. Coat. Technol.* **2014**, *238*, 68–74. [CrossRef]
19. Bartsch, M.; Marci, G.; Mull, K.; Sick, C. Fatigue testing of ceramic thermal barrier coatings for gas turbine blades. *Adv. Eng. Mater.* **1999**, *1*, 127–129. [CrossRef]
20. Bartsch, M.; Baufeld, B.; Dalkilic, S.; Chernova, L.; Heinzelmann, M. Fatigue cracks in a thermal barrier coating system on a superalloy in multiaxial thermomechanical testing. *Int. J. Fatigue* **2008**, *30*, 211–218. [CrossRef]
21. Hernandez, M.T.; Karlsson, A.M.; Bartsch, M. On TGO creep and the initiation of a class of fatigue cracks in thermal barrier coatings. *Surf. Coat. Technol.* **2009**, *203*, 3549–3558. [CrossRef]
22. Hernandez, M.T.; Cojocaru, D.; Bartsch, M.; Karlsson, A.M. On the opening of a class of fatigue cracks due to thermo-mechanical fatigue testing of thermal barrier coatings. *Computat. Mater. Sci.* **2011**, *50*, 2561–2572. [CrossRef]

23. Siddiqui, S.F.; Knipe, K.; Manero, A.; Meid, C.; Wischek, J.; Okasinski, J.; Almer, J.; Karlsson, A.M.; Bartsch, M.; Raghavan, S. Synchrotron X-ray measurement techniques for thermal barrier coated cylindrical samples under thermal gradients. *Rev. Sci. Instrum.* **2013**, *84*, 083904. [CrossRef] [PubMed]
24. Knipe, K.; Manero, A., II; Siddiqui, S.F.; Meid, C.; Wischek, J.; Okasinski, J.; Almer, J.; Karlsson, A.M.; Bartsch, M.; Raghavan, S. Strain response of thermal barrier coatings captured under extreme engine environments through synchrotron X-ray diffraction. *Nat. Commun.* **2014**, *5*, 4559. [CrossRef] [PubMed]
25. Manero, A., II; Sofronsky, S.; Knipe, K.; Meid, C.; Wischek, J.; Okasinski, J.; Almer, J.; Karlsson, A.M.; Raghavan, S.; Bartsch, M. Monitoring local strain in a thermal barrier coating system under thermal mechanical gas turbine operating conditions. *JOM* **2015**, *67*, 1528–1539. [CrossRef]
26. Weyant, C.; Almer, J.; Faber, K. Through-thickness determination of phase composition and residual stresses in thermal barrier coatings using high-energy X-rays. *Acta Mater.* **2010**, *58*, 943–951. [CrossRef]
27. Li, C.; Jacques, S.; Chen, Y.; Xiao, P.; Beale, A.; di Michael, M.; Markossan, N.; Nylen, P.; Cernik, R. Precise strain profile measurement as a function of depth in thermal barrier coatings using high energy synchrotron X-rays. *Scr. Mater.* **2016**, *113*, 122–126. [CrossRef]
28. Welzel, U.; Ligot, J.; Lamparter, P.; Vermeulenb, A.C.; Mittemeijera, E.J. Stress analysis of polycrystalline thin films and surface regions by X-ray diffraction. *J. Appl. Crystallogr.* **2005**, *38*, 1–29. [CrossRef]
29. Gladden, J.; So, J.H.; Maynard, J.; Saxe, P.; Page, Y.L. Reconciliation of ab initio theory and experimental elastic properties of Al_2O_3. *Appl. Phys. Lett.* **2004**, *85*, 392–394. [CrossRef]
30. Manns, T.; Scholtes, B. DECcalc-A program for the calculation of diffraction elastic constants from single crystal coefficients. *Mater. Sci. Forum Trans. Tech. Publ.* **2011**, *681*, 417–419. [CrossRef]
31. Whitaker, S. Forced convection heat transfer correlations for flow in pipes, past flat plates, single cylinders, single spheres, and for flow in packed beds and tube bundles. *AIChE J.* **1972**, *18*, 361–371. [CrossRef]
32. Abraham, J.; Sparrow, E.; Tong, J. Heat transfer in all pipe flow regimes: laminar, transitional/intermittent, and turbulent. *Int. J. Heat Mass Transf.* **2009**, *52*, 557–563. [CrossRef]